Departure from Navier-Stokes hydrodynamics in confined liquids

Karl P. Travis, B. D. Todd,* and Denis J. Evans
Research School of Chemistry, Australian National University, Canberra, Australian Capital Territory 0200, Australia
(Received 18 November 1996)

In this work we use nonequilibrium molecular dynamics (NEMD) to simulate an atomic liquid undergoing gravity-fed flow down a narrow channel. We compare the simulation results against the predictions of classical Navier-Stokes theory for two different channel widths. For a channel width of 5.1 molecular diameters, we find that the velocity profile deviates significantly from the hydrodynamic prediction. The shape of this velocity profile is found to be independent of the applied field (pressure gradient). We find that the heat flux profile does not agree with the cubic profile predicted by Navier-Stokes hydrodynamics, but shows significant oscillations located about one molecular diameter from the walls. This result differs from the earlier work of Todd and Evans [B. D. Todd and D. J. Evans, J. Chem. Phys. **103**, 9804 (1995)], in which an assumption of a purely quadratic velocity profile resulted in very weak oscillations in the heat flux. We find that in narrow channels the viscosity cannot be described by a linear, local constitutive relation. However, classical Navier-Stokes behavior is approached for a channel width of $>\sim 10$ molecular diameters. [S1063-651X(97)09504-4]

PACS number(s): 03.40.Gc, 66.20.+d, 47.55.Mh, 05.70.Ln

I. INTRODUCTION

Classical Navier-Stokes hydrodynamics is known to describe macroscopic flows of simple fluids. In situations where the state variables of temperature and density vary appreciably on a scale comparable to the molecular mean free path, these equations break down [1]. We therefore cannot expect the Navier-Stokes equations to accurately describe flow through very narrow channels or pores. Further complications arise when the fluid contains molecules that can rotate about their respective centers of mass.

In this paper we examine the limitations of the Navier-Stokes hydrodynamic solutions for a fluid undergoing gravity-fed flow down a square channel (Poiseuille flow). We examine in detail the streaming velocity profiles, heat flux, stress profile, and density profiles for a model fluid confined to channels with widths of 5.1 and 10.2 molecular diameters. We concern ourselves only with a simple fluid (i.e., one composed of structureless molecules). The case of molecular flow has been examined by us in another publication [2].

Recently, Todd and Evans [3] carried out simulations of a simple fluid undergoing planar Poiseuille flow in narrow channels. While they observed significant oscillations in the density and stress profiles, the heat flux and velocity profiles were essentially classical. This latter observation of a classical velocity profile for a channel only 5.1 molecular diameters wide does not agree with the theoretical predictions of Bitsanis *et al.* [1]. In the present paper we carry out much longer simulations which yield much better statistics and we use a recently developed technique [4] that allows the calculation of thermodynamic quantities to an extremely high spatial resolution.

*Present address: Cooperative Research Centre for Polymers, CSIRO Division of Chemicals and Polymers, Private Bag 10, Rosebank MDC, Clayton, Victoria 3169, Australia.

Navier-Stokes hydrodynamics for gravity-fed flow

Consider a gravity-driven flow between closely spaced parallel plates whose normals are perpendicular to the direction in which gravity acts. In this case the equation of motion is

$$\rho \frac{d\mathbf{u}}{dt} = -\nabla \cdot \mathbf{P} + n\mathbf{F}_e, \tag{1}$$

where the magnitude of the external field, $\mathbf{F}_e$, is simply the molecular mass of the fluid particles, m, multiplied by the acceleration due to gravity, g. The number density is n, $\mathbf{u}$ is the streaming velocity, and $\mathbf{P}$ is the pressure tensor. In writing Eq. (1) we have assumed that the vertical height of the plates is sufficiently small that the difference in hydrostatic pressure between the top and bottom of the plates may be ignored. For an isotropic fluid the pressure tensor $\mathbf{P}$ can be decomposed into a viscous part and an equilibrium part, $\mathbf{P}=\mathbf{\Pi}+p\mathbf{1}$, where $\mathbf{\Pi}$ is the viscous pressure tensor, $\mathbf{1}$ is the isotropic second rank tensor, and p is the scalar hydrostatic pressure.

In this special case of gravity-driven flow, at a steady state we have

$$\frac{d\Pi_{yx}(y)}{dy} = nF_e, \tag{2}$$

where we have chosen our x axis to be parallel to the external force and the y axis to be parallel to the normal of the plates. For a fluid with no spatial variations in the density, the shear stress profile will be linear. In reality, the presence of solid walls and a nonuniform temperature profile results in variations in the density across the channel, yielding a nonlinear stress profile.

The linear constitutive equation relating the shear stress to the shear viscosity is

$$\mathbf{\Pi}^{os} = -2\eta(\nabla \mathbf{u})^{os}, \tag{3}$$

where η is the shear viscosity, $\nabla \mathbf{u}$ is the strain rate tensor and the superscript os denotes the traceless symmetric part of the tensor. Combining Eqs. (2) and (3) with the assumption that the flow velocity takes the form $\mathbf{u}=[u_x(y),0,0]$, we have

$$\eta \frac{d^2 u_x(y)}{dy^2} = -nF_e, \tag{4}$$

which is a Navier-Stokes equation for the special case of steady planar gravity-fed flow. Equation (4) contains the assumption that the shear viscosity does not vary in space or time. Solving Eq. (4) for the flow velocity with stick boundary conditions gives the classical quadratic profile for Poiseuille flow

$$u_x = -\frac{h^2 n F_e}{2\eta}(\overline{y^2}-1), \tag{5}$$

where h is the half width of the channel and $\overline{y}$ is y/h. This expression is expected to break down for channels which are only a few molecular diameters wide.

The equation of change for the specific internal energy (energy continuity equation) is

$$\rho \frac{dU}{dt} = -\nabla \cdot \mathbf{J}_q - \mathbf{P}^T : \nabla \mathbf{u}, \tag{6}$$

where U is the specific internal energy, $\mathbf{J}_q$ is the heat flux vector, and $\mathbf{P}^T$ is the transpose of the pressure tensor. For gravity-fed flow in a square channel, at a steady state we have

$$\frac{dJ_{qy}(y)}{dy} = -\Pi_{yx}(y)\gamma(y), \tag{7}$$

where $\gamma = du_x(y)/dy$ is the strain rate. Equation (7) demonstrates that in the classical case the heat flux across the channel should be a cubic polynomial.

II. METHOD

A. Simulation details

We have previously described in detail the NEMD techniques used to simulate planar Poiseuille flow [3,5,6] and here only briefly outline the way in which the simulations were carried out. In our simulations we apply a constant force in the x direction to each particle, which has the same effect as allowing gravity to initiate the flow of fluid down the channel. The geometry of the system is shown in Fig. 1. Both the fluid and wall particles interact via the WCA interatomic potential function $\phi(r)$: $\phi(r)=4(r^{-12}-r^{-6})+1$, for $r<2^{1/6}$; $\phi(r)=0$, for $r>2^{1/6}$ (we have defined the WCA potential constants σ and ε to be unity for simplicity; we also define the fluid and wall particle masses to be unity). Henceforth, all quantities will be quoted in reduced units.

The system is surrounded by periodic images of itself in each of the three Cartesian dimensions. We note here that the simulation geometry is such that the external field is in the x direction and the heat flow is in the y direction. We examine two channel widths, $W=5.1$ and 10.2. Here W is defined as the separation in the y direction between the centers of the first layer of wall atoms adjacent to the fluid. Both systems

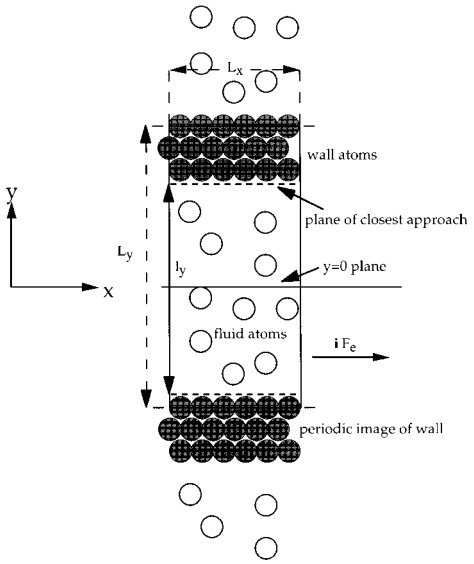

FIG. 1. Simulation geometry for planar Poiseuille flow. The z axis is normal to the page.

consisted of 360 fluid atoms bound by 216 wall atoms which were three atomic layers thick (72 atoms per layer).

The wall atoms were fixed in an fcc lattice structure by a combination of harmonic restoring forces [7] (with a spring constant set to 150.15) and a constraint mechanism that fixed the center of mass of each layer of wall particles while allowing individual wall atoms the freedom to vibrate about their lattice sites. There is only one three-atom-thick wall per simulation cell. The second wall was simply the periodic image of the first wall. This periodicity also ensures that the total density of the system remains constant. For details of the governing equations of motion and the integrating scheme used to solve them, the reader is referred to Refs. [5,6].

The average number density of both systems is $n=N/V=0.715$, where N is the number of liquid atoms and V is the volume accessible to the liquid. The unit cell dimensions, L_x, L_y, L_z for the $W=5.1$ channel are 10.8200, 7.2706, 10.8200, respectively, while for the $W=10.2$ channel they are 7.1905, 12.3844, 7.1905. It is important to note that L_y includes the fluid and wall particles (see Fig. 1). We observe that there is no unique average density of the fluid because there is no unambiguous definition of the total volume which is ''accessible'' to the fluid, and we again refer the reader to Refs. [5,6] for a discussion of this point. We simply note here that an effective channel width was found to be 4.3 for the $W=5.1$ system and 9.5 for the $W=10.2$ system.

The walls of both systems were kept at a constant temperature of 0.722 and density of 0.85. The wall temperature was held constant by application of a Gaussian thermostat, which ensured that the average temperature of all the wall atoms was constant.

For the channel width of 5.1 we studied the system at four different values of the magnitude of the external field, $F_e=0.05$, 0.10, 0.15, 0.20. For the $W=10.2$ system we chose a value of the field which yielded the same mean temperature that the $F_e=0.1$ simulation for the $W=5.1$ system did. This enabled us to make a direct comparison between the two different channel width simulations. The appropriate value of

the field was determined by Todd and Evans [3] to be $F_e=0.02471$. Once steady state was achieved with the external field switched on, production runs consisting of between 2 and 20 million steps were carried out with a reduced time step, $\tau=0.001$.

B. Calculation of the profiles

The streaming velocity can be obtained from the momentum current density $\mathbf{J}(\mathbf{r},t)$. The momentum current density for a system of identical particles is given microscopically by [8]

$$\mathbf{J}(\mathbf{r},t)\equiv\rho\mathbf{u}(\mathbf{r},t)=\sum_i m\mathbf{v}_i\delta(\mathbf{r}-\mathbf{r}_i(t)), \tag{8}$$

where the mass density $\rho(\mathbf{r},t)$ is given by

$$\rho(\mathbf{r},t)=\sum_i m\,\delta(\mathbf{r}-\mathbf{r}_i(t))\equiv mn(\mathbf{r},t), \tag{9}$$

where $n(\mathbf{r},t)$ is the number density at position $\mathbf{r}$ and time t. The streaming velocity is then simply

$$\mathbf{u}(\mathbf{r},t)=\frac{\Sigma_i m\mathbf{v}_i(t)\,\delta(\mathbf{r}-\mathbf{r}_i(t))}{\Sigma_i m\,\delta(\mathbf{r}-\mathbf{r}_i(t))}. \tag{10}$$

In practice, one replaces the Dirac delta function with a narrow step function that is nonzero only for a small range of separations. For a system such as ours we could divide the simulation cell into a number of slabs of thickness Δ_y and compute the streaming velocity as an average evaluated at the midpoint of each slab. This is the simple histogram method. While it is convenient to use and simple to implement, it suffers from the drawback that the slabwidth must be sufficiently large to contain enough particles to allow a good estimate of the average streaming velocity in a slab [9]. Thus there is a trade-off between lower statistical uncertainty and spatial resolution in the histogram method.

Recently, Daivis, Travis, and Todd [4] have proposed an alternative method of calculating microscopic quantities as a function of position, which is exact. In this method, one divides up the simulation cell into a number of equally spaced planes across the channel. One can then write for the x component of momentum current.

$$J_x(y,t)=\frac{1}{A}\sum_i m\dot{x}_i(t)\,\delta(y-y_i(t)), \tag{11}$$

where $A=L_xL_z$ is the area of an xz plane. Since $\delta(y-y_i(t_{\alpha(i)}))=\delta(t-t_{\alpha(i)})/|\dot{y}_i(t_{\alpha(i)})|$ we can obviously write

$$\delta(y-y_i(t))=\sum_{t_{\alpha(i)}}\frac{g\,d(t-t_{\alpha(i)})}{|\dot{y}_i(t_{\alpha(i)})|}, \tag{12}$$

where $\{t_{\alpha(i)}\}$ are the times α at which the y coordinate of particle i is equal to y. Substituting Eq. (12) into Eq. (11) we find that

$$J_x(y,t)=\frac{1}{A}\sum_i\sum_{t_{\alpha(i)}}\frac{m\dot{x}_i(t)\,\delta(t-t_{\alpha(i)})}{|\dot{y}_i(t_{\alpha(i)})|}. \tag{13}$$

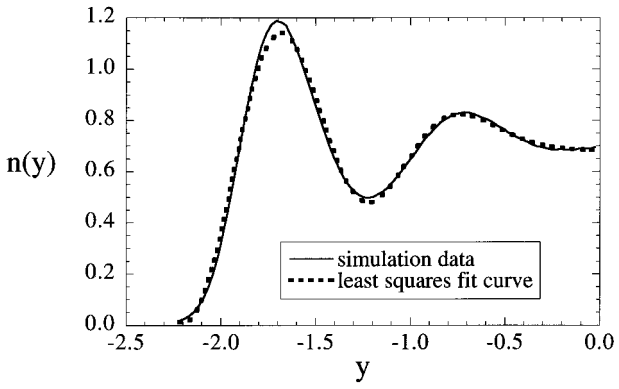

FIG. 2. Symmetrized number density profile for the 5.1 channel width system (solid line) and the least-squares fit of Eq. (15) to the data (broken line). The external field magnitude $F_e=0.1$. Statistical uncertainties are smaller than the plot symbols.

Assuming the system properties are stationary in time, we integrate Eq. (13) from time zero to τ and perform a time average:

$$\overline{J_x}(y)=\lim_{\tau\to\infty}\frac{1}{\tau A}\sum_i\sum_{0<t_{\alpha(i)}<\tau}\frac{m\dot{x}_i(t_{\alpha(i)})}{|\dot{y}_i(t_{\alpha(i)})|}. \tag{14}$$

The y component of the velocity of particle i at the precise time of the plane crossing is evaluated by first solving for $t_{\alpha(i)}$, the time at which plane α is crossed, by using a Newton-Raphson scheme and then predicting the velocity of the atom at this time. It is straightforward to calculate the density and kinetic-energy profiles using this method and hence the streaming velocity and kinetic-temperature profiles. We shall henceforth refer to this method of calculating the densities of hydrodynamic quantities as the planes calculation of kinetic properties (PKP). The statistical uncertainties in the PKP method are independent of the plane spacing. Using this method we are able to use a fine resolution in calculating the profiles.

III. RESULTS AND DISCUSSION

A. Number density and stress

The number density profile $n(y)$ is plotted in Fig. 2. We observe that the density is zero at $y=\pm2.25$ so we regard the data outside the range $-2.25<y<+2.25$ as being the wall density. We reject all data outside this range in our later analysis. We find that the data can be represented by a Fourier cosine series requiring only nine terms,

$$n(y)=a_0+\sum_{n=1}^{8}a_n\cos\frac{2\pi n}{1_y}y. \tag{15}$$

Figure 2 shows the number density calculated at planes together with the least-squares fit to Eq. (15).

The stress profile $\Pi_{yx}(y)$ can be calculated by at least two different methods. One can use the method of planes (MoP) [5], which involves evaluating an exact statistical mechanical expression for the stress at a plane, or by integrating the momentum continuity equation (IMC) [5]. Using the IMC method, Eq. (2) shows that the stress profile is given by

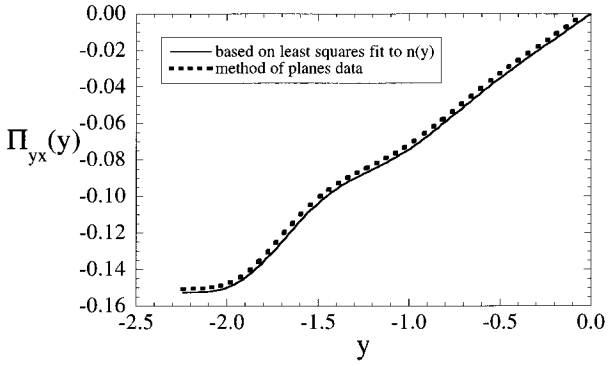

FIG. 3. $\Pi_{yx}(y)$ profile (obtained from integrating the number density profile) for the 5.1 channel width system (solid line) and the stress calculated via the method of planes (broken line). The external field magnitude $F_e=0.1$. Statistical uncertainties are smaller than the plot symbols.

$$\Pi_{yx}(y)=F_e\int_0^y n(y')dy'+C \tag{16}$$

where C is an integration constant whose value is determined by the fact that the stress is zero at the center of the channel. Assuming a density profile as in Eq. (15), we can evaluate the integral in Eq. (16) analytically to obtain

$$\Pi_{yx}(y)=F_e\left[a_0 y+\frac{1_y}{2\pi}\sum_{n=1}^{8}\frac{a_n}{n}\sin\frac{2\pi n}{1_y}y\right], \tag{17}$$

Figure 3 shows the stress calculated using Eq. (17) and that evaluated directly using the MoP. We see that within the statistical uncertainties, both methods yield identical stress profiles.

B. Velocity and strain rate profiles

The velocity profile is obtained by taking the ratio of the momentum density $J_x(y)$ and the mass density $\rho(y)$, both of which have been calculated using the PKP method. Figure 4 shows the symmetrized velocity profile obtained from the $F_e=0.1$ simulation. The crosses are the least-squares fit of the data to a quadratic equation of the form $\mathbf{u}_{\rm fit}=ay^2-b$ [we

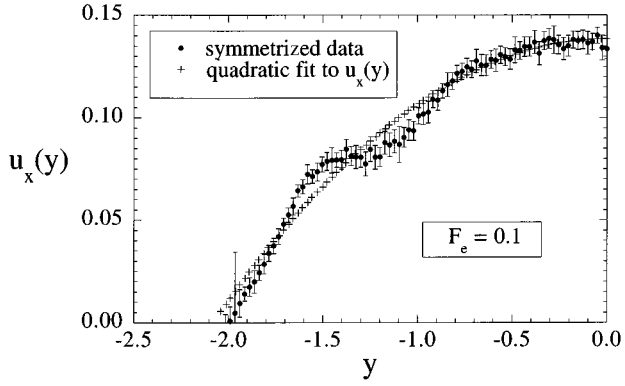

FIG. 4. Symmetrized streaming velocity profile for the 5.1 channel width system with $F_e=0.1$ (full circles) together with the least-squares fit of a quadratic equation to these data (crosses).

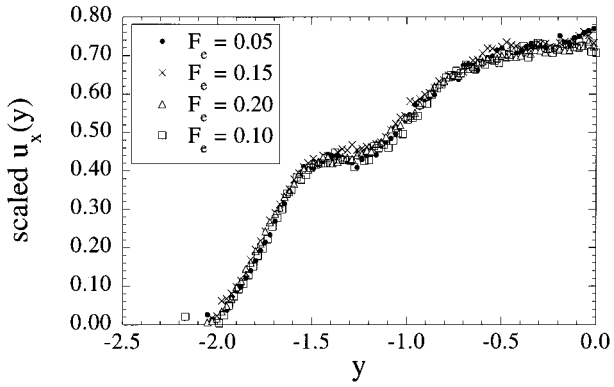

FIG. 5. Normalized streaming velocity profiles for the 5.1 channel width system at different external field magnitudes: $F_e=0.05$, 0.1, 0.15, 0.20. The profiles have been normalized by their integrals (see Table I).

note that true classical behavior would suggest $\mathbf{u}_{\rm fit}=a(y^2-1)$ but the use of rough walls in our simulation modifies the boundary conditions such that two parameters are required]. It is clear from Fig. 4 that the velocity profile deviates significantly from the hydrodynamic prediction. The general shape of the velocity profile agrees with the profiles obtained by Bitsanis *et al.* [1] at a roughly similar channel width. Figure 5 shows a plot of four symmetrized, normalized velocity profiles obtained from simulations at four different values of the external field. The profiles are normalized by dividing the result at each data point by the integral of the whole profile. Within the statistical uncertainties, all four profiles collapse into a single universal profile. This suggests that the shape of the profile is independent of the external field, at least within the linear regime. The normalizing factors are displayed in Table I. For the first three values of F_e, the areas under each profile are independent of the field magnitude, but at the highest field, there is a small but significant difference. Figure 6 shows the velocity profile obtained from the 10.2-channel-width simulation. Here we see that the data can be fit quite well with a quadratic curve. The oscillations in the profile are still present but they are extremely weak in comparison to the ones in the 5.1-channel-width profiles. The oscillations in the velocity profile are therefore a function of the channel width, at low fields.

To calculate the strain-rate profile $\gamma(y)$, we differentiate the velocity profile with respect to the y coordinate. Differentiating Eq. (5) gives the classical Navier-Stokes strain rate as

TABLE I. Integral of the velocity profile tabulated for different values of the external field.

F_e	$\int_{-2.25}^{2.25}u_z(y)dy$	$\int_{-2.25}^{2.25}u_z(y)dy/F_e$
0.05	0.1900	3.8
0.10	0.38	3.8
0.15	0.59	3.9
0.20	0.82	4.1

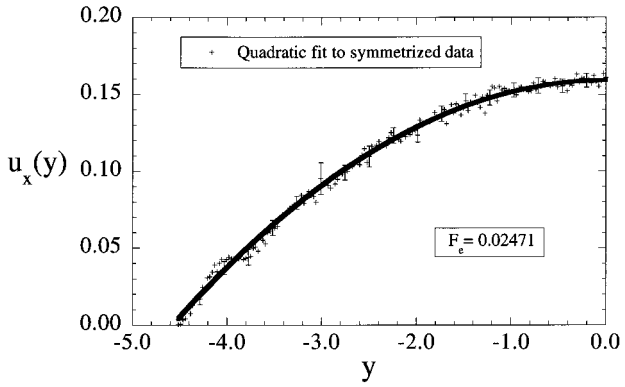

FIG. 6. Symmetrized streaming velocity profile for the 10.2 channel width system with $F_e=0.02471$ (crosses) together with the least-squares fit of a quadratic equation to the data (solid line).

$$\gamma(y)=\frac{-nF_e y}{\eta}, \tag{18}$$

which is linear in y. Since our calculated velocity profiles are not quadratic in y it is clear that we will not obtain a linear strain-rate profile.

To obtain a smooth strain-rate profile, we have fitted the velocity profile from the $F_e=0.1$ simulation to a function which consists of a term quadratic in y and a cosine series.

$$u_x(y)=b_1+b_2y^2+\sum_{n=1} a_n \cos\frac{2\pi n}{1_y}y, \tag{19}$$

where the a's and b's represent the least-squares-fit coefficients. We find that eight cosine terms are sufficient to represent the data. Figure 7 shows the velocity profile obtained from the $F_e=0.1$ simulation together with the quadratic fit to this velocity profile (QVP) and the fit defined in Eq. (19) [we shall denote this as the quadratic-plus-cosine-series fit (QCVP)]. The data has been symmetrized prior to the least-squares-fit procedure. Again we find a reasonably good fit to the data.

Differentiating Eq. (19), we have an analytic expression for the strain rate:

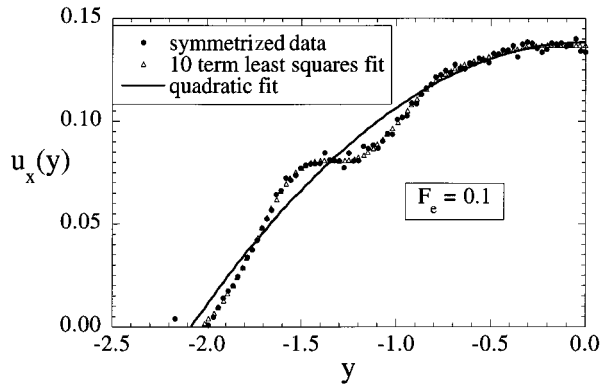

FIG. 7. Comparison of two fitting functions with the streaming velocity data for the 5.1 channel width system at an external field $F_e=0.1$. The fitting functions are a quadratic form (solid line) and a function composed of a quadratic part and a Fourier cosine series [Eq. (19), open triangles in figure].

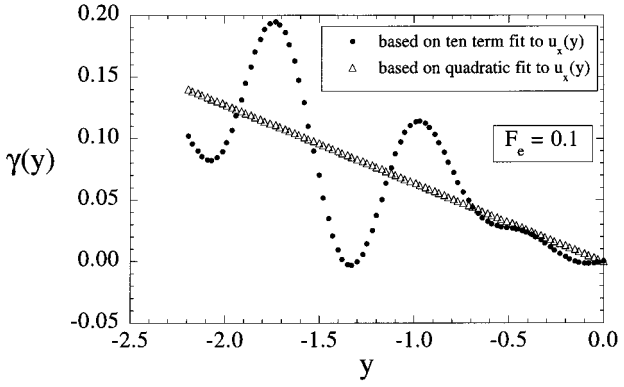

FIG. 8. Strain-rate profile $\gamma(y)$ derived by assuming a quadratic velocity profile (open triangles) and by assuming a velocity profile that can be represented by a function composed of a quadratic part plus a Fourier cosine series (full circles). The channel width is 5.1 and the external field $F_e=0.1$.

$$\gamma(y)=2b_2y-\frac{2\pi}{1_y}\sum_{n=1}^{8} n\ a_n \sin\frac{2\pi n}{1_y}y. \tag{20}$$

Figure 8 shows the resulting curve fit to the strain rate data and a strain-rate profile calculated by assuming that the streaming velocity can be fitted to a simple quadratic form as predicted by Navier-Stokes hydrodynamics. The curve representing Eq. (20) shows oscillations across the channel and is significantly different from the Navier-Stokes prediction. The wavelength of these variations in the strain rate is of the order of a particle diameter.

C. Streaming kinetic energy

The peculiar kinetic-energy density at a plane can be written as

$$K^{\text{pec}}(y)=\frac{1}{2A}\sum_i m_i(\mathbf{v}_i-\mathbf{u}(\mathbf{r}_i))^2\delta(y-y_i(t)), \tag{21}$$

where the streaming velocity, $\mathbf{u}(\mathbf{r}_i)$ must be known in order to calculate this kinetic energy. This can be determined by assuming a form for $\mathbf{u}$, minimizing the total instantaneous peculiar kinetic energy, Eq. (21), with respect to the coefficients used to fit $\mathbf{u}$ [8,10] and using these instantaneous values to calculate an instantaneous peculiar kinetic energy (hardwired method). In the case of the Poiseuille flow simulations, previous work [3,5,6] had assumed that $\mathbf{u}_x(y)$ was of the form $\mathbf{u}_x(y)=a+by^2$, which, in the case of large channel widths, is a justified choice. Alternatively, we may calculate the kinetic-energy density in the laboratory frame,

$$K^{\text{lab}}(y)=\frac{1}{2A}\sum_i m_i\mathbf{v}_i^2\delta(y-y_i(t)), \tag{22}$$

and then subtract the streaming component afterwards. The streaming kinetic-energy density is given macroscopically by $\frac{1}{2}\rho\mathbf{u}\cdot\mathbf{u}$. The advantage of this second method is that it makes no assumptions about the form of the streaming velocity. Figure 9 shows a plot of the peculiar kinetic energy calculated directly via Eq. (21) and calculated by subtracting the streaming kinetic-energy density from the laboratory kinetic-

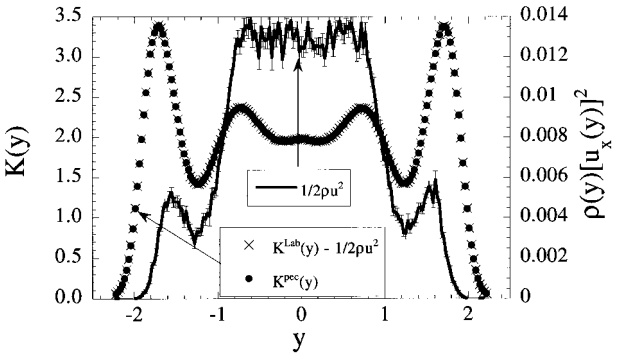

FIG. 9. Comparison of the laboratory and peculiar (assuming a quadratic velocity profile) kinetic energy profiles (left-hand axis) and the streaming kinetic energy, $\frac{1}{2}\rho\mathbf{u}^2$ (right-hand axis). The channel width is 5.1 and the external field $F_e=0.1$.

energy density. For comparison, we also show the streaming kinetic-energy density (right axis). The two versions of the peculiar kinetic energy are virtually identical (statistical uncertainties are too small to display). Note the small magnitude of the streaming (convective) kinetic-energy density. This convective component is of the order 10^{-2}. We therefore expect that at higher fields the two versions of the peculiar kinetic-energy density will differ more substantially.

D. The heat flux vector

The heat-flux vector, like the stress, may be obtained via two different methods, the method-of-planes route [6] and a mesoscopic route which involves integrating the energy continuity equation IEC method) [3,6]. With the IEC method, integrating Eq. (7) gives the expression for the heat flux as

$$J_{qy}(y)=-\int_0^y dy'\,\Pi_{yx}(y')\,\gamma(y')+C', \tag{23}$$

where the constant of integration, C', is determined by the requirement that the heat flux be zero in the center of the channel. Weak-flow Navier-Stokes hydrodynamics predicts a purely cubic dependence of the heat-flux vector across the channel. Figure 10 shows the heat-flux vector calculated us-

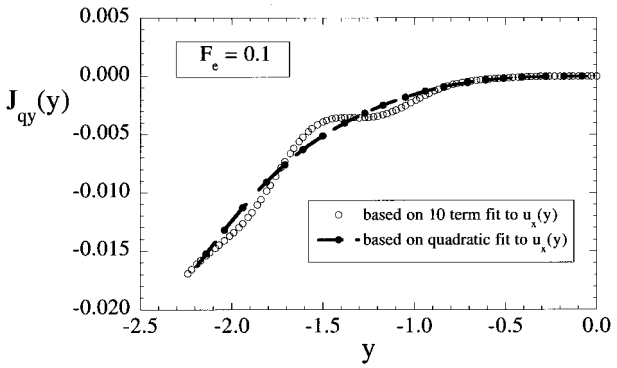

FIG. 10. The heat flux $J_{qy}(y)$ obtained by the IEC method. The broken line is the heat flux calculated on the assumption that the velocity profile is classical, i.e., quadratic, while the filled circles are the heat flux calculated from a strain rate based on the derivative of Eq. (19). The channel width is 5.1 and the external field $F_e=0.1$.

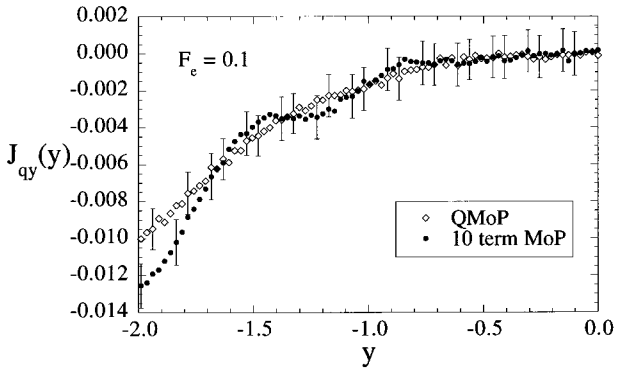

FIG. 11. MoP heat flux calculated using a streaming velocity which is determined by assuming a quadratic form (QMoP) and one which is calculated by assuming it has a functional form composed of a quadratic part plus a Fourier cosine series (filled circles). The channel width is 5.1 and the external field $F_e=0.1$.

ing Eq. (23) with two different strain-rate profiles, one based on a quadratic fit to the velocity profile (QVP), the second based on Eq. (19) (QCVP). From the figure, we see that there are significant oscillations in the heat-flux vector when calculated using a strain rate derived from the QCVP fit. In order to verify this functional form for the heat flux, we have calculated the heat flux directly from an exact statistical mechanical expression (MoP) [6]. However, the MoP calculation of the heat flux suffers from an obvious drawback. The streaming velocity evaluated at planes appears in the expression for the heat-flux vector in both the kinetic contribution and the potential contribution [6]. Direct calculation therefore requires *a priori* knowledge of the instantaneous streaming velocity. Todd, Daivis, and Evans [6] used a quadratic estimate for the instantaneous streaming velocity at a plane. This choice for the streaming velocity was justified because they simulated a wide channel which yielded classical Navier-Stokes behavior. However, this work has shown that in narrow channels the streaming velocity deviates significantly from quadratic behavior. We have made the assumption that the streaming velocity can be estimated by Eq. (19) and used the least-squares method to determine the expansion coefficients instantaneously. Figure 11 shows the heat-flux vector obtained using MoP where two different assumptions for the form of $\mathbf{u}_x(y)$ have been used. We see that when $\mathbf{u}_x(y)$ is assumed to be quadratic, an essentially cubic heat flux results, whereas when $\mathbf{u}_x(y)$ is assumed to be of the form of Eq. (19) the oscillations are recovered. Within the statistical uncertainties, the MoP heat flux agrees with that calculated via the IEC method (Fig. 12).

E. Viscosity profile

The shear viscosity η is assumed to be independent of position in the weak-flow Navier-Stokes theory of liquids. Todd and co-workers [3,5] found that the shear viscosity of a simple fluid undergoing planar Poiseuille flow is not constant across the channel, but exhibits strong oscillations. They calculated the shear viscosity profile from the *local* linear constitutive relation,

$$\eta(y)=\frac{-\Pi_{yx}(y)}{\gamma(y)}, \tag{24}$$

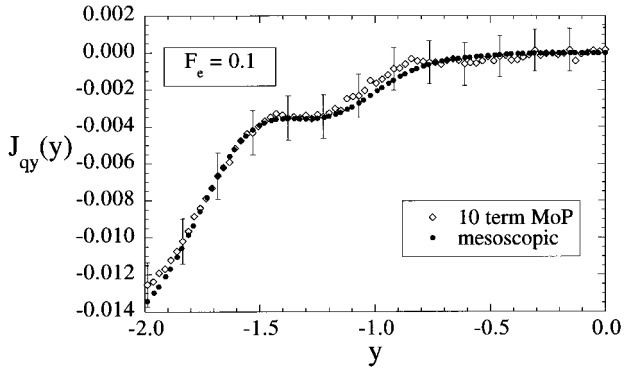

FIG. 12. Comparison of the heat flux $J_{qy}(y)$ obtained using the direct Method of Planes route, and that obtained indirectly using the IEC method [both methods assume either directly or indirectly that the streaming velocity can be approximated by Eq. (19)]. The channel width is 5.1 and the external field $F_e=0.1$.

but assumed a strain rate based on a quadratic fit to their velocity profiles. However, for a channel width of 5.1, we have shown that this assumption is no longer valid. We have calculated a shear viscosity profile from Eq. (24) using our derived strain-rate profile. We find that the viscosity diverges due to the fact that the strain rate goes to zero at $y\sim-1.3$, (see Fig. 8) but the shear stress remains nonzero (see Fig. 3). This shows that a local linear constitutive relation cannot give an adequate relation between the stress and strain-rate fields in these narrow channels. If viscosity is a nonlocal function of y, a nonlocal generalization of the linear constitutive relation relating the stress to the strain rate is required. Such a relation is

$$\Pi_{yx}(y) = -\int_0^y \eta(y;y-y')\,\gamma(y')\,dy'. \qquad (25)$$

However, we do not have sufficient data to calculate the viscosity kernel.

IV. CONCLUSIONS

We have used nonequilibrium molecular dynamics to simulate an atomic liquid undergoing gravity-fed flow down a narrow channel. Our model fluid is spatially inhomogeneous and it is expected that for such a system, the Navier-Stokes equations will break down. Todd and Evans [3] have recently carried out similar calculations for a fluid confined to channels widths of 5.1 and 10.2 molecular diameters. Surprisingly, they found general agreement with the Navier-Stokes theory despite the strong oscillations in the density profile. Our work differs from that of Todd and Evans [3] in that we have used higher resolution and longer simulations to enable the calculation of the density, velocity, heat-flux, and strain-rate profiles with high statistical precision. For a channel width of 5.1 molecular diameters we find that the velocity profile deviates significantly from the Navier-Stokes hydrodynamic prediction. Except for the highest field strength, the shape of this velocity profile is found to be independent of the applied field (see Table I). At a channel width of 10.2 molecular diameters, classical Navier-Stokes behavior is approached.

We have fitted our velocity profiles using a function that consists of a classical (quadratic) part plus a Fourier cosine series. Using this fit, we then derived a strain-rate profile that is found to deviate significantly from the classical linear form. Similarly, we use a Fourier cosine series to fit the number density profile. With this fit we derive a stress profile by integrating the momentum continuity expression. The stress profile so derived agrees well with the exact statistical mechanical route to the stress calculated using the MoP devised by Todd and co-workers [3,5,6]. By integrating the energy continuity expression we derive a heat flux which for narrow channels deviates from the classical cubic behavior predicted by Navier-Stokes theory and the earlier results of Todd and co-workers [3,6]. We find that the heat flux has oscillations located at roughly the same points as those in the velocity profiles. We use the method-of-planes technique to calculate an ''exact'' expression for the heat flux. The MoP heat flux is found to agree with the mesoscopically derived heat flux. We must stress here that the statistical mechanical definition of the heat flux requires a knowledge of the streaming velocity evaluated at a plane. The analytic form for this streaming velocity is not known *a priori*. The best one can do is to try to find a set of appropriate expansion functions and fit the coefficients by a least-squares procedure. Our results suggest that our choice of expansion functions is reasonable, within the degree of the statistical accuracy of our data.

In their earlier work, Todd and co-workers [3,5] calculated the viscosity of a fluid undergoing planar Poiseuille flow in a narrow channel. They found that this transport coefficient was not constant across the channel as required by the Navier-Stokes theory, but instead exhibited strong oscillations. We find that the use of the local constitutive relation for shear viscosity gives an absurd viscosity profile. Our results, therefore, suggest that for this narrow channel width, the viscosity is a nonlocal function of position across the channel.

ACKNOWLEDGMENT

We wish to thank the Australian National University Supercomputer Facility for a generous grant of computer time on the University's FUJITSU supercomputers.

[1] I. Bitsanis, T. K. Vanderlick, M. Tirrel, and H. T. Davis, J. Chem. Phys. **89**, 3152 (1988).
[2] K. P. Travis and D. J. Evans, Phys. Rev. E **55**, 1566 (1997).
[3] B. D. Todd and D. J. Evans, J. Chem. Phys. **103**, 9804 (1995).
[4] P. J. Daivis, K. P. Travis, and B. D. Todd, J. Chem. Phys. **104**, 9651 (1996).
[5] B. D. Todd, D. J. Evans, and P. J. Daivis, Phys. Rev. E **52**, 1627 (1995).

[6] B. D. Todd, P. J. Daivis, and D. J. Evans, Phys. Rev. E **51**, 4362 (1995).
[7] J. G. Powles, S. Murad, and P. V. Ravi, Chem. Phys. Lett. **188**, 21 (1992).
[8] D. J. Evans and G. P. Morriss, *Statistical Mechanics of Non-equilibrium Liquids* (Academic, London, 1990).
[9] S. Y. Liem, D. Brown, and J. H. R. Clarke, Phys. Rev. A **45**, 3706 (1992).
[10] K. P. Travis, P. J. Daivis, and D. J. Evans, J. Chem. Phys. **103**, 10 638 (1995).